Deletion of osteopontin or bone sialoprotein induces opposite bone responses to mechanical stimulation in mice

M. Maalouf, H. Çinar, W. Bouleftour, M. Thomas, A. Vanden-Bossche, N. Laroche, M.T. Linossier, S. Peyroche, M.H. Lafage-Proust, L. Vico, et al.

Deletion of Osteopontin or Bone Sialoprotein induces opposite bone responses to mechanical stimulation in mice

M. Maalouf[1], H. Çinar[1], W. Bouleftour[2], M. Thomas[1], A. Vanden-Bossche[1], N. Laroche[1], M. T. Linossier[1], S. Peyroche[1], M. H. Lafage-Proust[1], L. Vico[1], A. Guignandon[1], L. Malaval[1].

[1]LBTO, INSERM, U1059-SAINBIOSE, Université de Lyon, Université Jean Monnet, Saint-Etienne, France
[2]Hôpital Nord, University Hospital, Université Jean Monnet, Saint-Etienne, France.

Running title: OPN, BSP and bone mechanical stimulation

Corresponding author:

Dr Mathieu Maalouf

LBTO, INSERM, U1059-SAINBIOSE

Université de Lyon - Université Jean Monnet

Pôle Santé Nord - Faculté de Médecine, Rm 118

10 Chemin de la Marandière

F 42270 St Priest en Jarez, France

T: 33477421444

e-mail: mathieu.maalouf@univ-st-etienne.fr

Supplementary Information added to the submission:

- 5 Supplementary Tables

Abstract

Aim

Osteopontin (OPN) and Bone Sialoprotein (BSP) are co-expressed in bone and display overlapping and complementary physiological properties. Both genes show a rapid expression response to mechanical stimulation. We used mice with single and double deletions (DKO) of BSP and OPN to assess the specificity of their roles in skeletal adaptation to loading.

Methods

Two month old Wild-Type (WT), BSP knockout ($BSP^{-/-}$), $OPN^{-/-}$ and DKO male mice were submitted to two mechanical stimulation regimen respectively impacting trabecular bone (Hypergravity, HG) and cortical bone (Whole Body Vibration, WBV).

Results

HG increased trabecular bone volume (BV/TV) in WT femur through reduced resorption, and in $BSP^{-/-}$ mice femur and vertebra through increased bone formation. In contrast, HG increased the turnover of $OPN^{-/-}$ bone, resulting in reduced femur and vertebra BV/TV. HG did not affect DKO bones. Similarly, WBV increased cortical thickness in $BSP^{-/-}$ mice and decreased it in $OPN^{-/-}$, without affecting structurally WT and DKO bone. Vibrated $BSP^{-/-}$ mice displayed increased endocortical bone formation with a drop in Sclerostin expression, and reduced periosteal osteoclasts with lower Rankl and Cathepsin K expression. In contrast, vibrated $OPN^{-/-}$ endocortical bone displayed decreased formation and increased osteoclast coverage.

Conclusion

Therefore, under two regimen (HG and WBV) targeting distinct bone compartments, absence of OPN resulted in bone loss while lack of BSP induced bone gain, reflecting divergent structural adaptations. Strikingly, absence of both proteins led to a relative insensitivity to either mechanical

challenge. Interplay between OPN and BSP thus appears as a key element of skeletal response to mechanical stimulation.

Key words: Bone Sialoprotein, Hypergravity, Knockout, Osteopontin, Whole Body Vibration.

Introduction

Osteopontin (OPN) and Bone Sialoprotein (BSP) are two non-collagenous proteins present in the bone matrix and involved in bone formation, resorption and mineralization processes.[1,2] Together with Matrix Extracellular Phosphoglycoprotein (MEPE), Dentin Matrix Protein-1 (DMP1) and Dentin Sialophosphoprotein (DSPP), OPN and BSP form the SIBLING (Small Integrin Binding Ligand N-linked Glycoproteins), a family of phylogenetically related extracellular matrix components whose genes are aligned on the same chromosome (4 in human, 5 in mouse).[3,4] In a 129sv/CD1 mouse genetic background (wild-type, WT) single gene knockouts of BSP ($BSP^{-/-}$,[5]), OPN ($OPN^{-/-}$), as well as a double knockout ($BSP^{-/-}$ + $OPN^{-/-}$ = DKO,[6]) have been developed and/or characterized in our group. We generated DKO mice because of the evidence of a functional compensation between BSP and OPN in the anabolic bone response to Parathyroid Hormone (PTH) [7] and because $BSP^{-/-}$ mice over-express OPN protein in bone tissue and in blood.[8] Interestingly, all three genetic conditions ($BSP^{-/-}$, $OPN^{-/-}$ and DKO) affect trabecular and cortical bone architecture and dynamics in distinct ways.[6]

OPN and BSP have been shown in many *in vitro* and *in vivo* models to be rapidly and temporarily (hours or days) expressed by bone cells in response to mechanical stimulation,[9–13] which makes them early markers of bone's perception of loading. To our knowledge, only one study reported the effect of increased mechanical loading on $OPN^{-/-}$ mice and showed in calvaria sutures a delay in formation activity under tensile mechanical stress.[14] No study to date has investigated the effects of loading on other bone compartments of $OPN^{-/-}$, $BSP^{-/-}$ or DKO mice. To evaluate the role of these proteins and their interactions under mechanical challenge, we tested WT, $BSP^{-/-}$, $OPN^{-/-}$ and DKO mice in two different mechanical stimulation challenges: hypergravity (HG) and whole body vibration (WBV). Our laboratory has previously described the impact of HG and WBV on the skeleton of C57Bl/6 growing mice. In these studies, each challenge displayed structural effects

targeting a specific bone compartment. Under a 2G acceleration, HG increased trabecular bone mass[15] whereas WBV (at 2G and 90Hz) accelerated cortical bone accrual.[16] In the present study, this compartment specificity allowed us to assess the impact of mechanical stimulation on mice with mutations affecting both trabecular and cortical bone.[6]

Our results show that under both HG and WBV, the absence of OPN results in bone loss, the absence of BSP induces or potentiates bone gain while in the absence of both proteins (DKO) no bone architectural change is observed under either challenge. These findings highlight a strong interaction between OPN and BSP in the bone response to mechanical stress.

Results

Hypergravity induces trabecular bone loss in OPN$^{-/-}$ mice, in contrast to bone gain in WT and BSP$^{-/-}$ mice

Only WT mice showed a (~10%) reduction of their final weight under HG (Table S2). At 2G, WT and BSP$^{-/-}$ mice increased their trabecular bone volume (BV/TV: +27% for both, Figure 2B) and trabecular thickness (Tb.Th: +11% for WT and +9% for BSP$^{-/-}$, Figure 2D) in the distal femoral metaphysis with the addition of an increase of connectivity density only for BSP$^{-/-}$ mice (Conn. D: +23%, Figure 2E). Strikingly, OPN$^{-/-}$ mice lost femoral trabecular BV/TV (-27%), and Conn.D (-20%) under HG, with no change for the DKO (Figure 2B, D, E). Similar effects of HG were observed in L2 vertebra for all genotypes except the WT, which showed no bone gain under HG, highlighting the greater overall response of BSP$^{-/-}$ mice (Figure 2C, Table S2). No effect of HG on cortical parameters was observed for any genotype (Table S2).

Hypergravity effects on bone cellular activities are genotype-specific

In WT trabecular bone, HG decreased significantly osteoclast surfaces (Oc.S/BS), with no significant change in bone formation rate (BFR/BS, Figure 3A, C). Nonetheless, RT-qPCR analysis of the tibial trabecular compartment of WT mice showed increased OSX, OCN and ALP expression under 2G (Figure 3D, Table S3). HG increased trabecular bone remodeling in OPN$^{-/-}$ mice, with higher BFR/BS and Oc.S/BS (Figure 3A, C) as well as increased OSX, ALP, OCN and TRAcP expression (Figure 3D, Table S3). BSP$^{-/-}$ mice showed a specific increase in BFR/BS with no change in Oc.S/BS (Figure 3A, B) with an increased expression of ERα (Figure 3D). DKO mice showed no significant change in bone cellular activity or mRNA expression under HG (Figure 3A, D, Table S2, S3).

Whole body vibration induces cortical bone loss in OPN$^{-/-}$ mice, in contrast to bone gain in BSP$^{-/-}$ mice

WBV did not affect body weight in any genotype (Table S4). No structural change was observed in the cortical bone of VB WT and DKO mice (Figure 4, Table S4). VB OPN$^{-/-}$ mice displayed significant decrease of cortical thickness (Ct.Th: -9%), cortical area (Ct.Ar: -13%) and total area (Tt.Ar: -9%, Figure 4A). In contrast, BSP$^{-/-}$ mice showed a significant increase in Ct.Th (+7%) under WBV (Figure 4A), with a trend towards a decrease of the Ma.Ar/Tt.Ar ratio (p=0.061, Table S4) and no change in Tt.Ar (Figure 4A), indicative of a narrowing medullary space under WBV. VB OPN$^{-/-}$ mice showed a reduction in polar moment of inertia (pMOI, Figure 4A), Imax/Cmax and Imin/Cmin (Table S4), reflecting a modification of bone mass distribution likely to impact biomechanical properties. The local cortical thicknesses analysis showed an uneven thinning of cortical bone in VB OPN$^{-/-}$ mice, mostly located in the anterolateral and posterolateral sectors, while cortical thickening in VB BSP$^{-/-}$ mice occurred in all sectors except the lateral (Figure 4B).

Of note, OPN$^{-/-}$ was the only genotype to show a structural effect on trabecular bone under WBV, with a reduction of BV/TV (vertebra) and/or trabecular quality (smaller trabecular number (Tb.N), higher trabecular separation (Tb.Sp), smaller Conn.D in VB femur, Table S4).

Whole body vibration induces opposite cellular responses in OPN$^{-/-}$ and BSP$^{-/-}$ cortical bones

WBV did not affect significantly formation and resorption parameters in endocortical and periosteal surfaces of WT and DKO mice (Figure 5A). Vibrated OPN$^{-/-}$ mice showed a decrease in endocortical formation (Ec.BFR/BPm: -54%, Figure 5A, 6; Table S4) and in periosteal mineral apposition rate (MAR: -21%, Figure 5B, 6), in line with a trend towards decreased OCN expression (p=0.062, Table S5). This went with an increase of endocortical resorption in OPN$^{-/-}$ mice under

WBV (Ec.Oc.Pm/BPm: +95%, Figure 5A, 6). Vibrated $BSP^{-/-}$ mice increased bone formation activity both on the endocortical (Figure 5A, 6) and periosteal surfaces (Figure 5B, 6) with additionally a drop in SCLN expression (Figure 5C). $BSP^{-/-}$ mice also showed a decrease in periosteal Oc.Pm/BPm (-68%, Figure 5B, 6A) with a drop in RANKL and Cath K expression in cortical bone under WBV (Figure 5C).

Discussion

The rapid and transient increase in gene expression of OPN and BSP under mechanical stimulation has been amply documented.[9–13] The variations in expression of either protein observed in the different genotypes under both challenges (Tables S3, S5) reflect here long term temporal kinetics, independent of this early response. As far as we know, no studies to date tested BSP-deficient mice under mechanical stimulation. Moreover, due to the complex functional interactions between OPN and BSP that we highlighted in previous studies,[6–8] the DKO model was critical here to assess the interplay between OPN and BSP under mechanical challenge.

The bone phenotypes of the 4 mouse lines used in this study have been extensively described (). Briefly, the trabecular BV/TV of the distal femur in $BSP^{-/-}$ and $OPN^{-/-}$ mice is similar to WT at 2 months (the start of our experiments) and increases to values higher than WT (~+25%) in mature, 4 month-old mice (). DKO mice have lower values (-30%) at 2 months that reach WT values by 4 months (). At the end of our experiments (3.5 months of age), $OPN^{-/-}$ and $BSP^{-/-}$ values were already higher than WT (only in trend for $BSP^{-/-}$ femur in the 1G group, Tables S2, S4). $BSP^{-/-}$ mice are characterized by thinner cortices than WT, while $OPN^{-/-}$ cortical bone is thicker (). DKO cortical bone has the same average Ct.Th as WT in the midshaft area assessed, but presents remarkable macro-porosities in the posterior part of the midshaft (). This was observed at the end of our experiments (Tables S2, S4) with, in addition, no difference between genotypes in biomechanically relevant parameters such as pMOI, Imax, Imin, Imax/Cmax and Imin/Cmin (Table S4).

The present study shows that the single extinction of OPN or BSP affects the response of bone to mechanical stimulation in opposite ways, while their concomitant absence results in no structural effects. These findings were made with two different mechanical stress protocols, which mainly affect trabecular bone (HG,[15]) or mainly target cortical bone (WBV,[16]).

Our group previously reported an increase of trabecular BV/TV under HG in C57Bl/6 mice, associated with a drop of osteoclast surfaces,[15] that we confirm here on WT 129sv/CD1 outbred mice, in which increased bone formation marker expression also suggests a stimulation of osteogenesis (Figure 3D). This contrasts with the response of $OPN^{-/-}$ mice which show a drop in trabecular BV/TV with increased turnover under HG. Intriguingly, $OPN^{-/-}$ was the only genotype to increase osteoclast surfaces under both protocols (HG and WBV) in all the bone compartments investigated by histomorphometry. Historically, $OPN^{-/-}$ mice have been shown to be resistant to bone loss induced by hindlimb unloading (tail suspension) or ovariectomy, in part due to impaired stimulation of osteoclast activity.[17,18] Our results indicate that the defect in $OPN^{-/-}$ osteoclast sensitivity can be rescued by mechanical stress. All this suggests that OPN has a pivotal role in the sensitivity and/or response of osteoclasts to variations in the mechanical environment. That $OPN^{-/-}$ mice also display a decrease of bone formation parameters in the cortical compartment under WBV indicates that the mutation also affects the osteoblast response. In line with the delayed formation activity under tensile mechanical stress in $OPN^{-/-}$ calvarial sutures reported by [14], our results suggest a mechanoprotective function for OPN in bone. Interestingly such a role has been described in the kidney, where OPN protects against the deleterious mechanical effects of glomerular hypertension on podocytes through its attachment to the αV integrin.[19,20] Similarly, bone cells grown from $OPN^{-/-}$ long bones display a defective production of nitric oxide (NO), a mediator of osteoblast mechanotransduction,[21] under pulsatile fluid flow.[22]

In $BSP^{-/-}$ mice, the increase in trabecular BV/TV under HG concerned both femur and vertebra. Of note, trabecular BV/TV is higher than WT at both sites in 1G $BSP^{-/-}$ mice, indicating that the response to HG is not a mere adjustment of bone mass to the new mechanical environment. Under HG, $BSP^{-/-}$ mice increased their trabecular BFR/BS, and molecular data from the endosteal (including the trabecular) compartment showed a higher ERα expression. ERα role in mechanotransduction has been described as pro-osteogenic,[23] inducing osteoblastic maturation

through the upregulation of mitochondrial cytochrome c oxidase (COX) 1 mRNA and more globally by improving cellular ATP synthesis.[24,25]

WBV did not accelerate the cortical growth of our WT mice, in contrast to (Gnybkin et al.), likely because of the different age of the animals at the start of the experiment (2 months vs 7 weeks in Gnybkin et al.), as well as the different genetic backgrounds. However, and in contrast to $OPN^{-/-}$, $BSP^{-/-}$ mice under WBV did show an increase in cortical thickness. Surprisingly, VB $BSP^{-/-}$ mice, in addition to an increased global bone formation in cortical bone, associated with a drop of sclerostin expression, also decreased their periosteal resorption activity, which at baseline (in $BSP^{-/-}$ CT) is the highest of all 4 genotypes. This correlated with decreased cortical expression of RANKL and CathK. We have previously shown that in contrast to WT, $BSP^{-/-}$ mice do not increase cortical thickness under intermittent Parathyroid Hormone (iPTH) administration.[26] WBV is indeed the only known experimental challenge to increase Ct.Th in $BSP^{-/-}$ mice, suggesting a specific role of BSP in the skeletal response to mechanical stimuli.

Taking into account all the data obtained in HG and WBV, the contrast between $OPN^{-/-}$ mice losing and $BSP^{-/-}$ mice gaining bone is further emphasized by the fact that DKO mice did not display any significant structural change under either protocol. Also, DKO mice showed little or no change in cellular parameters, suggesting that the concomitant absence of OPN and BSP induces a relative insensitivity of osteoblast and osteoclast responses under mechanical stimulation. Clearly, the interactions between OPN and BSP appear to be a key element in the skeletal response to mechanical stress. More work will be needed to identify the specific cellular and molecular mechanisms of this cross-talk. In particular, a fine temporal analysis of the cortical response will be required to detail and quantify the kinetics of the anabolic or catabolic effects (or the lack thereof) observed under WBV, but also the impact on osteocytes in all genotypes including the DKO.

In summary, under two different whole body mechanical stress protocols, targeting distinct bone compartments, $BSP^{-/-}$ mice gain bone mass while $OPN^{-/-}$ mice lose bone. Absence of both proteins (DKO) leads to insensitivity to mechanical stress, at least in terms of final outcome and with the challenges used in this work. These results suggest that interplay between OPN and BSP is a key element of skeletal adaptation to mechanical stimulation.

Materials & Methods

Animal care

WT 129sv/CD1 mice, along with $BSP^{-/-}$, $OPN^{-/-}$ and DKO mice in the same genetic background were used in these experiments. $BSP^{-/-}$ mice have been generated by homologous recombination, as described.[5] $OPN^{-/-}$ and DKO mice were engineered through targeted deletion, using the Transcription Activator-Like Effector Nuclease (TALEN) technique on a $BSP^{+/-}$ background, as described.[6] For line maintenance and experimentation, the animals were housed and bred in the PLEXAN facility (Platform for Experiments and Analysis, Faculty of Medicine, University Jean Monnet, Saint-Etienne, France). Mice were kept at standard temperature (23±2°C), in a light-controlled environment (12 h light/12 h dark cycle) and were fed a standard pellet diet (SAFE A03, Safe, Augy, France) with water ad libitum. All animal experiments have been approved by the local ethical committee (Comité d'Ethique en Experimentation Animale de la Loire CEEAL-UJM, agreement Nr°98) and the Animal Welfare Committee of the PLEXAN. After screening by the CEEAL-UJM, HG experiments received approval from the national authority (Ministère de l'Enseignement Supérieur, de la Recherche et de l'Innovation, APAFIS Nr 8160-2016112415129882 v6). The procedures for the care and killing of the animals were in accordance with the European Community Standards on the care and use of laboratory animals (Ministère de l'Agriculture, France, Authorization Nr°42-18-0801).

Hypergravity regimen

The 1.4m radius centrifuge with four peripheral gondolas associated with an electronic control system (COMAT Aérospace, Flourens, France) is housed in the PLEXAN site ([15], Figure 1A). All gondolas are equipped with a camera-based monitoring system to track the behavior of the animals and the food/water stocks (Figure 1B). Two-month-old male mice of all 4 genotypes were separated

between controls, kept at normal gravity (1G), and a centrifuged group (n=10 mice/group). Cages of the 2G groups were transferred into the gondolas (10 mice/cage/gondola, Figure 1B) and the centrifuge was run at 2G acceleration for 3 weeks, with a weekly 5-minute stop to weigh the mice and renew food and water. Control cages were kept in the centrifuge room to homogenize environmental factors.

Whole body vibration regimen

Shaker platforms (TIRA Vibration Test Systems TV 52120, Schalkau, Germany) on which aluminum discs (30cm diameter, 4mm thickness) are attached were used to generate vibrations ([16], Figure 1C). The G-level was controlled by an accelerometer (PBB Piezotronics, 100mV/g, ref 352C33). Two-month-old male mice of all 4 genotypes were separated between controls (CT, n=10) and vibrated (VB, n=10). During each WBV session, all mice from the same cage were put on the shaker's disc and left free to move (Figure 1C). For VB mice, the plates were accelerated at 2G, at a 90 Hz frequency (sinusoidal signal) for 15 min/day, 5 day/week (Monday to Friday) during 6 weeks. CT mice were put on an inactive shaker for 15 minutes during the vibration sessions, alternating with the VB.

Tetracycline labelling and sample collection

In order to label bone formation surfaces, all mice were injected with 30 mg/kg tetracycline (TTC, Sigma-Aldrich) in saline solution, seven days and three days before killing. At the respective ends of HG and WBV experiments, all mice were euthanized and femora, vertebrae and tibiae were collected.

Microtomography

For microtomographic (µCT) analysis, formalin-fixed and ethanol dehydrated femur and second lumbar (L2) vertebra were scanned with a Viva CT40 tomograph (Scanco Medical, Bassersdorf, Switzerland) following standard guidelines.[27] Data were acquired at 55 keV with a 145 mA current

and a 10 µm isotropic cubic resolution. Three-dimensional reconstructions were generated using the following parameters: σ=1.2; support=2; threshold=245 for trabecular bone and 280 for cortical bone.

The structural parameters of trabecular bone, bone volume/trabecular volume (BV/TV), trabecular thickness (Tb.Th), trabecular number (Tb.N), trabecular separation (Tb.Sp), structure model index (SMI) and density of connections (Conn.D) were measured in a set of 150 sections above the distal growth plate of the femur and from all sections between the two growth plates of the L2 vertebra, within Regions of Interest (ROI) excluding primary bone,. The structural parameters of the femur midshaft, cortical thickness (Ct.Th), total cross sectional area (Tt.Ar), cortical area (Ct.Ar), marrow area (Ma.Ar), cortical porosity (Ct.Po), maximal (Imax) and minimal areal moment of inertia (Imin), polar moment of inertia (pMOI = Imax + Imin), maximal radius perpendicular to Imax direction (Cmax), minimal radius perpendicular to Imin direction (Cmin), section module (Imax/Cmax and Imin/Cmin) and tissue mineral density (TMD), as calibrated with an HAP phantom, were calculated by integration of the value on each transverse section of a set of 60, starting 500 sections (5 mm) above the distal growth plate. On the 30th section of each image stack, the cortical bone was compartmentalized into radial sectors separated by 45 degrees and the cortical thickness was manually measured in each sector with the µCT software.

Histomorphometry

After µCT analysis, femur bones were cut in two with a Dremel model 395 electric drill fitted with a diamond blade (Dremel Multipro, Breda, Netherlands) at the lower two-thirds of their length. Both parts were embedded separately in methyl-methacrylate.

The distal metaphysis was cut longitudinally with a tungsten-carbide-bladed microtome (Leica SM2500E, Wetzlar, Germany) to obtain 9 µm slices. Sections were stained with modified Goldner's trichrome or with tartrate-resistant acid phosphatase (TRAcP) histochemistry for

osteoclasts with Light-Green counterstain, or were left unstained. Bone formation was assessed on unstained sections by measuring single (sLs/BS) and double TTC labeled surfaces per bone surface (dLs/BS) and derive mineralizing surfaces per bone surface (MS/BS, in %, with MS = 0.5*sLs+dLs). The mineral apposition rate (MAR, in µm/day) was assessed as the distance between double labels. The bone formation rate per bone surface (BFR/BS, in $\mu m^3/\mu m^2$/day) was calculated as (MS/BS)*MAR. Osteoclast surfaces per bone surface (Oc.S/BS, in %), osteoclast number per bone perimeter (N.Oc/B.Pm) and osteoclast mean length (Oc.Le) were measured on TRAcP stained sections. Measurements excluded primary bone to fit with the ROI of µCT analysis. Results for each mouse are averages of 5 non-successive sections. Femur midshaft was cut transversely with a diamond-coated wire (Escil, Precision Diamond Wire Saw, Chassieu, France) into 300 µm slices. The bone formation parameters, mineralized perimeter per bone perimeter (MPm/BPm, in %), MAR and BFR per bone perimeter (BFR/BPm, $\mu m^2/\mu m$/d) were measured on one slice per mouse, taken within the µCT ROI. Measurements were made on the unstained and unmounted section, kept flat on a slide in a few drops of alcohol during analysis. The section was then gradually rehydrated, TRAcP-stained without counter-staining, mounted and re-analyzed for osteoclast perimeter per bone perimeter (Oc.Pm/BPm, %). Measurements were done on endocortical (Ec.) and periosteal surfaces (Ps.) separately, and on both sides of each slice, whose values were averaged.

Real-Time PCR

For quantitative real-time PCR analysis (RT-qPCR) of WBV cortical bone, collected tibiae were cleaned from connective tissue, their shafts were cut-out and flushed with sterile PBS to restrict the sampling to cortical bone, then crushed in liquid nitrogen with steel balls in a mixer mill (Sartorius, Gottingen, Germany) before extraction with Tri-Reagent (Sigma-Aldrich). For HG experiment, the tibia shafts were flushed with Tri-Reagent in order to best sample the trabecular compartment. RNA harvested with Tri-Reagent was purified on columns (Rneasy Plus Mini Kit, Qiagen, Hilden,

Germany), quantified with the Ribogreen kit (Invitrogen, Life Technologies, Eugene, OR, USA) and quality checked with an Experion automated electrophoresis station (Bio Rad, Hercules, CA, USA). Messenger RNA was reverse transcribed (iScript cDNA synthesis Kit, Biorad) and 400 ng of cDNA were amplified using the SYBR Green I dye (Lightcycler faststart DNA masterSYBR green I, Roche, Germany). Names and primer sequences of the genes of interest are given in Table S1. Expression of the housekeeping gene GAPDH did not vary significantly within or between groups (not shown).

Statistics

Inter-group comparisons were performed with Fisher's *t*-test whenever the conditions of normality (Shapiro-Francia test) and homoscedasticity (*F*-test) were verified (Figures 2, 4, S1 and S2). If not, the non-parametric Wilcoxon-Mann-Whitney *U*-test was used (Figures 3 and 5, Tables S2 to S5).

Data Availability Statement

The data that supports the findings of this study are available in the supplementary material of this article.

Acknowledgements

The small animal centrifuge is an open facility of the Centre National d'Etudes Spatiales (CNES, Paris, France). The authors thank the staff of the PLEXAN facility for skillful technical assistance, Dr Myriam Normand and Dr Bernard Roche (U1059, LBTO) for advice on statistics, Elisa Dalix for help with RT-qPCR and Dr Laura Peurière for help in HG mice sample harvesting.

Funding: The "Agence Nationale de la Recherche" (grants ANR-13-BSV1-0010-01 "Mouse_Kosto" to LM), the "Institut National de la Santé et de la Recherche Médicale" (INSERM), the "Université Jean Monnet" of Saint Etienne, and the "Ministère de l'Enseignement supérieur, de la Recherche et de l'Innovation" (PhD scholarship for Mathieu Maalouf).

Conflict of Interest

The authors declare no conflict of interest.

References

1. Ganss B, Kim RH, Sodek J. Bone sialoprotein. *Crit Rev Oral Biol Med Off Publ Am Assoc Oral Biol*. 1999;10(1):79-98. doi:10.1177/10454411990100010401

2. Sodek J, Ganss B, McKee MD. Osteopontin. *Crit Rev Oral Biol Med*. 2000;11(3):279-303. doi:10.1177/10454411000110030101

3. Fisher LW, Fedarko NS. Six Genes Expressed in Bones and Teeth Encode the Current Members of the SIBLING Family of Proteins. *Connect Tissue Res*. 2003;44(1):33-40. doi:10.1080/03008200390152061

4. Staines KA, MacRae VE, Farquharson C. The importance of the SIBLING family of proteins on skeletal mineralisation and bone remodelling. *J Endocrinol*. 2012;214(3):241-255. doi:10.1530/joe-12-0143

5. Malaval L, Wade-Guéye NM, Boudiffa M, et al. Bone sialoprotein plays a functional role in bone formation and osteoclastogenesis. *J Exp Med*. 2008;205(5):1145-1153. doi:10.1084/jem.20071294

6. Bouleftour W, Juignet L, Verdière L, et al. Deletion of OPN in BSP knockout mice does not correct bone hypomineralization but results in high bone turnover. *Bone*. 2019;120:411-422. doi:10.1016/j.bone.2018.12.001

7. Bouleftour W, Bouet G, Granito RN, et al. Blocking the Expression of Both Bone Sialoprotein (BSP) and Osteopontin (OPN) Impairs the Anabolic Action of PTH in Mouse Calvaria Bone: either BSP or OPN is required for PTH action. *J Cell Physiol*. 2015;230(3):568-577. doi:10.1002/jcp.24772

8. Granito RN, Bouleftour W, Sabido O, et al. Absence of Bone Sialoprotein (BSP) Alters Profoundly Hematopoiesis and Upregulates Osteopontin: lack of BSP alters bone marrow composition. *J Cell Physiol*. 2015;230(6):1342-1351. doi:10.1002/jcp.24877

9. Kreke MR, Huckle WR, Goldstein AS. Fluid flow stimulates expression of osteopontin and bone sialoprotein by bone marrow stromal cells in a temporally dependent manner. *Bone*. 2005;36(6):1047-1055. doi:10.1016/j.bone.2005.03.008

10. Mitsui N, Suzuki N, Maeno M, et al. Optimal compressive force induces bone formation via increasing bone sialoprotein and prostaglandin E2 production appropriately. *Life Sci*. 2005;77(25):3168-3182. doi:10.1016/j.lfs.2005.03.037

11. Terai K, Takano-Yamamoto T, Ohba Y, et al. Role of Osteopontin in Bone Remodeling Caused by Mechanical Stress. *J Bone Miner Res*. 1999;14(6):839-849. doi:10.1359/jbmr.1999.14.6.839

12. Yu H, Ren Y, Sandham A, Ren A, Huang L, Bai D. Mechanical Tensile Stress Effects on the Expression of Bone Sialoprotein in Bovine Cementoblasts. *Angle Orthod*. 2009;79(2):346-352. doi:10.2319/011508-20.1

13. Zhou S, Zu Y, Sun Z, Zhuang F, Yang C. Effects of Hypergravity on Osteopontin Expression in Osteoblasts. *PLOS ONE*. 2015;10(6):e0128846. doi:10.1371/journal.pone.0128846

14. Morinobu M, Ishijima M, Rittling SR, et al. Osteopontin Expression in Osteoblasts and Osteocytes During Bone Formation Under Mechanical Stress in the Calvarial Suture In Vivo. *J Bone Miner Res*. 2003;18(9):1706-1715. doi:10.1359/jbmr.2003.18.9.1706

15. Gnyubkin V, Guignandon A, Laroche N, et al. Effects of chronic hypergravity: from adaptive to deleterious responses in growing mouse skeleton. *J Appl Physiol*. 2015;119(8):908-917. doi:10.1152/japplphysiol.00364.2015

16. Gnyubkin V, Guignandon A, Laroche N, Vanden-Bossche A, Malaval L, Vico L. High-acceleration whole body vibration stimulates cortical bone accrual and increases bone mineral content in growing mice. *J Biomech*. 2016;49(9):1899-1908. doi:10.1016/j.jbiomech.2016.04.031

17. Ishijima M, Rittling SR, Yamashita T, et al. Enhancement of Osteoclastic Bone Resorption and Suppression of Osteoblastic Bone Formation in Response to Reduced Mechanical Stress Do Not Occur in the Absence of Osteopontin. *J Exp Med*. 2001;193(3):399-404.

18. Yoshitake H, Rittling SR, Denhardt DT, Noda M. Osteopontin-deficient mice are resistant to ovariectomy-induced bone resorption. *Proc Natl Acad Sci U S A*. 1999;96(14):8156-8160.

19. Schordan S, Schordan E, Endlich K, Endlich N. αV-Integrins mediate the mechanoprotective action of osteopontin in podocytes. *Am J Physiol-Ren Physiol*. 2011;300(1):F119-F132. doi:10.1152/ajprenal.00143.2010

20. Endlich N, Sunohara M, Nietfeld W, et al. Analysis of differential gene expression in stretched podocytes: osteopontin enhances adaptation of podocytes to mechanical stress. *FASEB J Off Publ Fed Am Soc Exp Biol*. 2002;16(13):1850-1852. doi:10.1096/fj.02-0125fje

21. Qin, Liu W, Cao H, Xiao G. Molecular mechanosensors in osteocytes. *Bone Res*. 2020;8(1):23. doi:10.1038/s41413-020-0099-y

22. Denhardt DT, Burger EH, Kazanecki C, Krishna S, Semeins CM, Klein-Nulend J. Osteopontin-Deficient Bone Cells Are Defective in Their Ability to Produce NO in Response to Pulsatile Fluid Flow. *Biochem Biophys Res Commun*. 2001;288(2):448-453. doi:10.1006/bbrc.2001.5780

23. Khalid AB, Krum SA. Estrogen receptors alpha and beta in bone. *Bone*. 2016;87:130-135. doi:10.1016/j.bone.2016.03.016

24. Galea GL, Meakin LB, Sugiyama T, et al. Estrogen Receptor α Mediates Proliferation of Osteoblastic Cells Stimulated by Estrogen and Mechanical Strain, but Their Acute Down-regulation of the Wnt Antagonist Sost Is Mediated by Estrogen Receptor β *. *J Biol Chem*. 2013;288(13):9035-9048. doi:10.1074/jbc.M112.405456

25. Wu GJ, Chen JT, Lin PI, Cherng YG, Yang ST, Chen RM. Inhibition of the estrogen receptor alpha signaling delays bone regeneration and alters osteoblast maturation, energy metabolism, and angiogenesis. *Life Sci*. 2020;258:118195. doi:10.1016/j.lfs.2020.118195

26. Wade-Gueye NM, Boudiffa M, Laroche N, et al. Mice Lacking Bone Sialoprotein (BSP) Lose Bone after Ovariectomy and Display Skeletal Site-Specific Response to Intermittent PTH Treatment. *Endocrinology*. 2010;151(11):5103-5113. doi:10.1210/en.2010-0091

27. Bouxsein ML, Boyd SK, Christiansen BA, Guldberg RE, Jepsen KJ, Müller R. Guidelines for assessment of bone microstructure in rodents using micro–computed tomography. *J Bone Miner Res*. 2010;25(7):1468-1486. doi:10.1002/jbmr.141

Figures Legends

Figure 1: Hypergravity and whole body vibration apparatus used for mechanical stimulation on mice. (A) For hypergravity experiment the centrifuge is composed of a central disc and four arms holding peripheral swinging gondolas. (B) The gondolas are designed to hold rodent cages and are equipped with a video monitoring system. (C) For whole body vibration experiments, the mice are placed on an aluminum disk that is attached to a shaker platform during the vibration session.

Figure 2: Effect of 2G hypergravity on the trabecular bone of the femoral distal metaphysis and the L2-vertebra of WT, OPN$^{-/-}$, BSP$^{-/-}$ and DKO mice. (A) 3D reconstruction images of femoral trabecular bone. (B) Femoral and (C) vertebral BV/TV, (D) femoral Tb.Th and (E) Conn.D. The graph gives p-values between genotype-matched 1G and 2G, in **bold** when <0.05, Fisher *t*-test (for C) or Mann-Whitney *U* test, N = 9-10 mice/group. See also Table S2.

Figure 3: Effect of 2G hypergravity on trabecular cellular activities and molecular markers in long bones of WT, OPN$^{-/-}$, BSP$^{-/-}$ and DKO mice. (A) Bone formation activity (BFR/BS) and osteoclast surfaces (Oc.S/BS), (B) Tetracyclin labelling and (C) TRAcP staining of the femur distal metaphysis at the end-point of the experiment, white arrows indicate trabecular double labeling surfaces in BSP$^{-/-}$ mice. (D) Marker mRNA expression in the tibial bone shaft, given as ratio to the housekeeping gene GAPDH. The graphs gives *p* values between genotype-matched 1G and 2G, in **bold** when <0.05, Mann-Whitney *U* test, N = 5-10 mice/group. See also Tables S2 and S3.

Figure 4: Effect of WBV on the femoral cortical bone of WT, OPN$^{-/-}$, BSP$^{-/-}$ and DKO mice. (A) Cortical thickness (Ct.Th), cortical area (Ct.Ar), total area (Tt.Ar) and polar moment of inertia (pMOI) of control (CT) and vibrated (VB) mice. The graph gives p-values between genotype-matched CT and VB, in **bold** when <0.05, Mann-Whitney *U* test, N = 9-10 mice/group. See also Table S4. (B) Effect of WBV on local femoral cortical bone thickness in OPN$^{-/-}$ and BSP$^{-/-}$ mice. The graphs show the percent variation of VB vs CT in each sector (mean±SD), for OPN$^{-/-}$ (yellow bars) and BSP$^{-/-}$ mice (red bars). *: $p<0.05$, **: $p<0.01$, ***: $p<0.001$ vs CT, Fisher's *t*-test, N = 9-10 mice/group. The schematics on the right summarize the targeted effects of WBV on OPN$^{-/-}$ (loss in yellow areas) and BSP$^{-/-}$ cortical bone (gain in red areas).

Figure 5: Effect of WBV on cortical cellular activities in the femur of WT, OPN$^{-/-}$, BSP$^{-/-}$ and DKO mice. (A) endocortical and (B) persioteal MAR, BFR/BPm and Oc.Pm/BPm in the cortical

bone of control (CT) and vibrated (VB) mice. (C) Marker mRNA expression in femur cortical bone of WT, $OPN^{-/-}$, $BSP^{-/-}$ and DKO mice. Values are given as ratio to GAPDH. The graphs gives *p* values between genotype-matched CT and VB, in **bold** when <0.05, Mann-Whitney *U* test, N = 5-10 mice/group. See also Table S4.

Figure 6: Site-targeted effect of WBV on $OPN^{-/-}$ and $BSP^{-/-}$ cortical bone. Tetracycline labeling and TRAcP staining of osteoclasts in the same section of $OPN^{-/-}$ and $BSP^{-/-}$ cortical bone from control (CT) and vibrated (VB) mice; bars = 250 µm; white arrows: formation surfaces, blue arrows: osteoclast surfaces. Abbreviations: TTC: tetracycline; TRAcP: tartrate-resistant acid phosphatase; Ec: endocortical surface; Ps: periosteal surface.

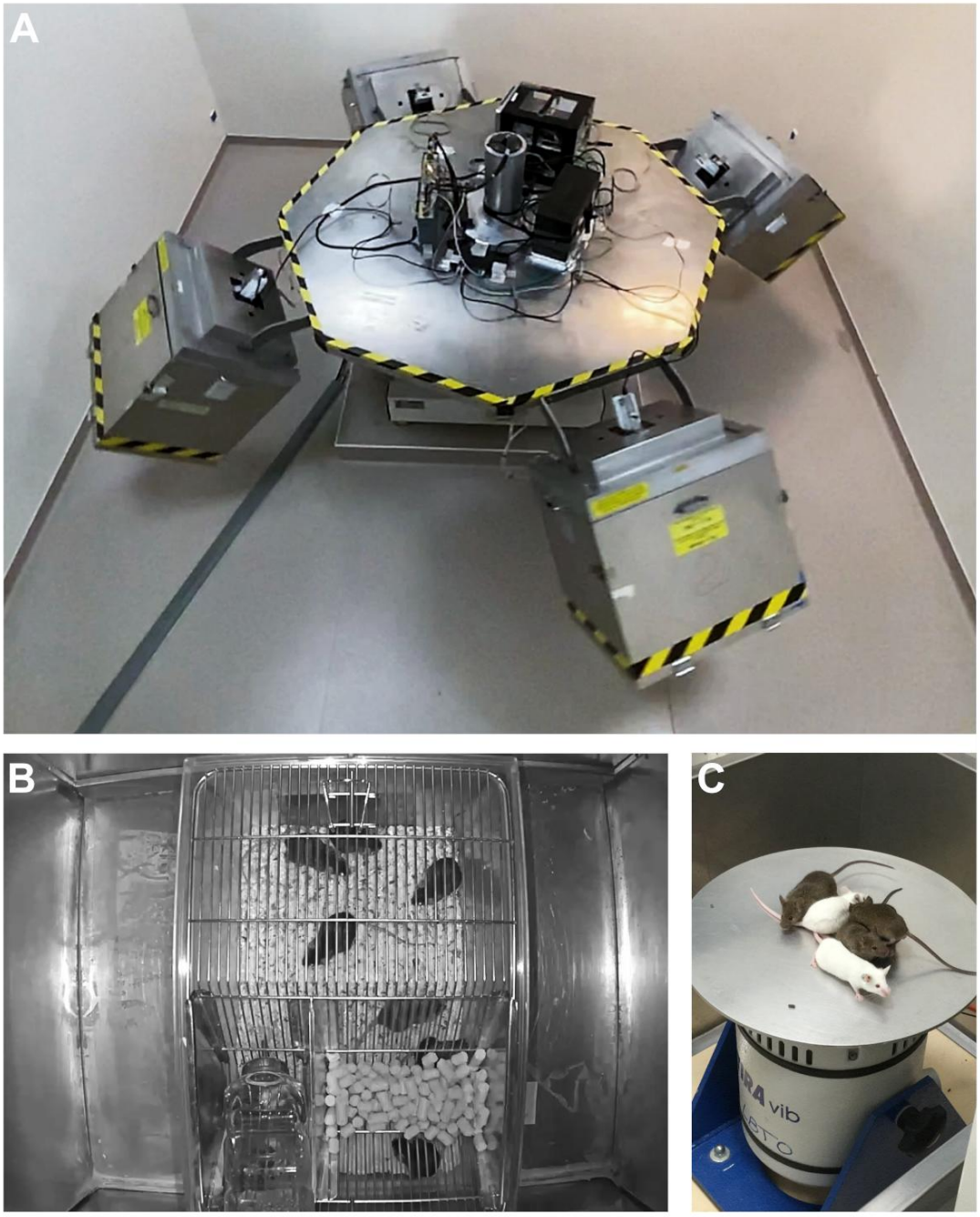

Maalouf et al., Figure 1

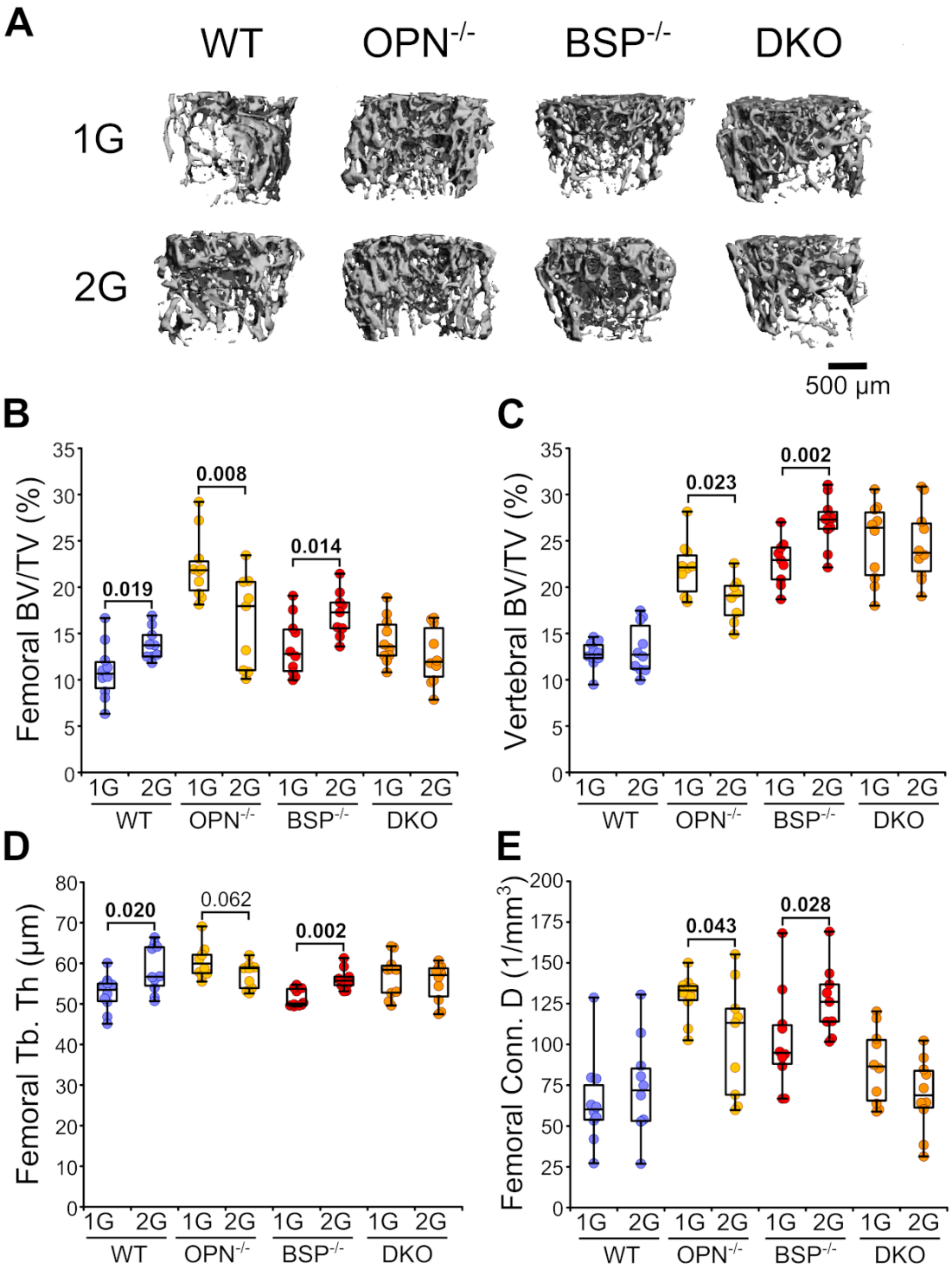

Maalouf et al., Figure 2

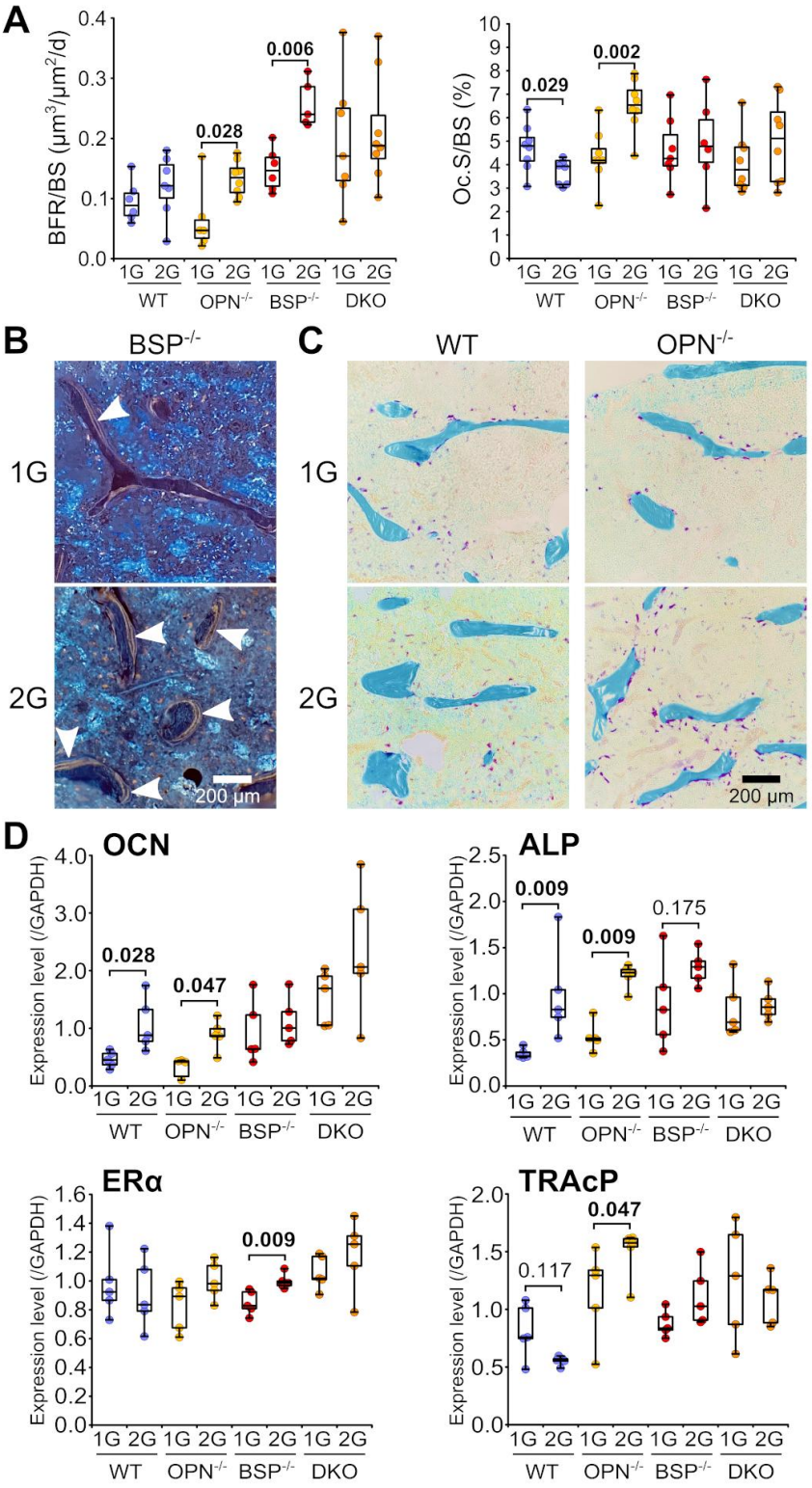

Maalouf et al., Figure 3

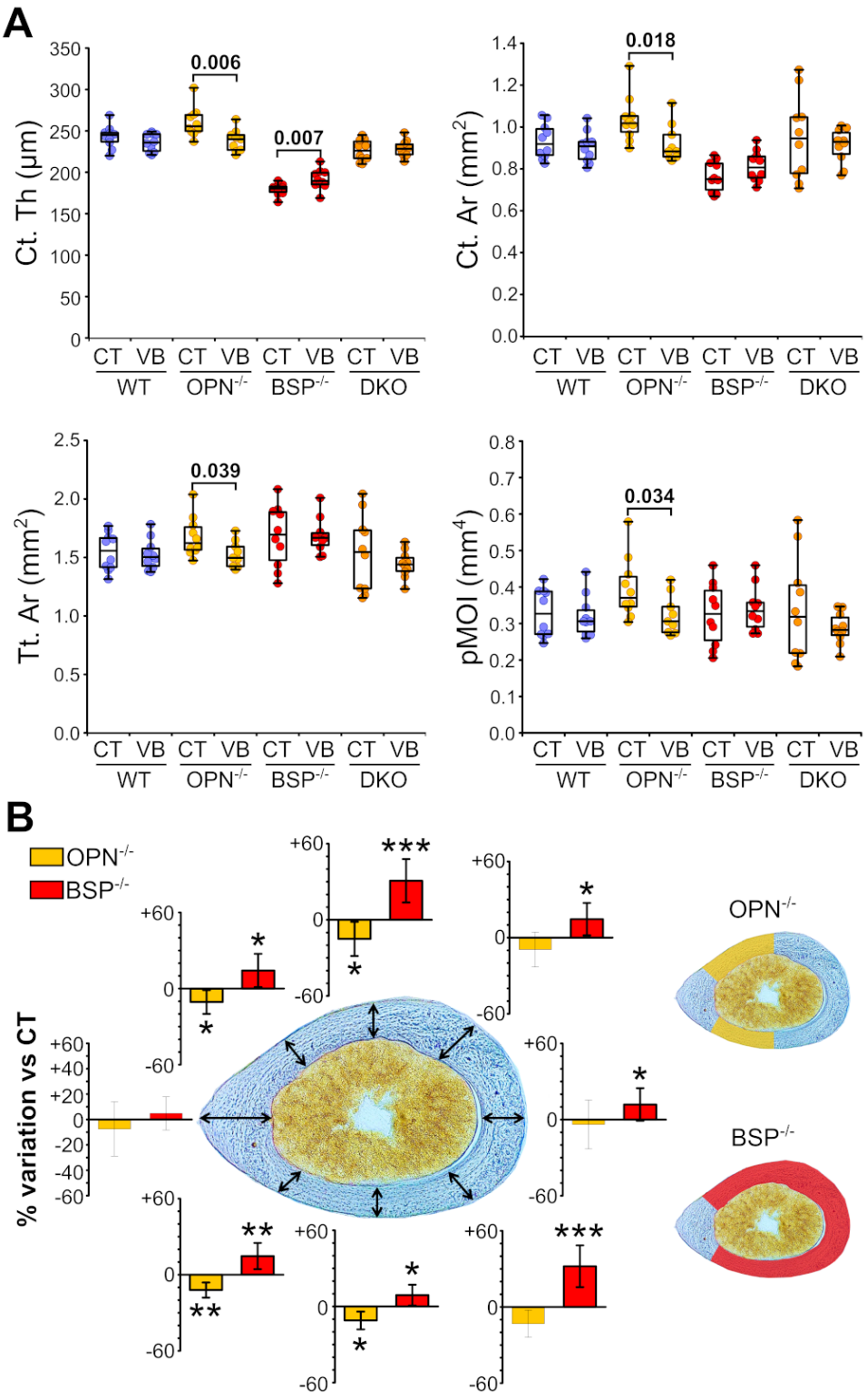

Maalouf et al., Figure 4

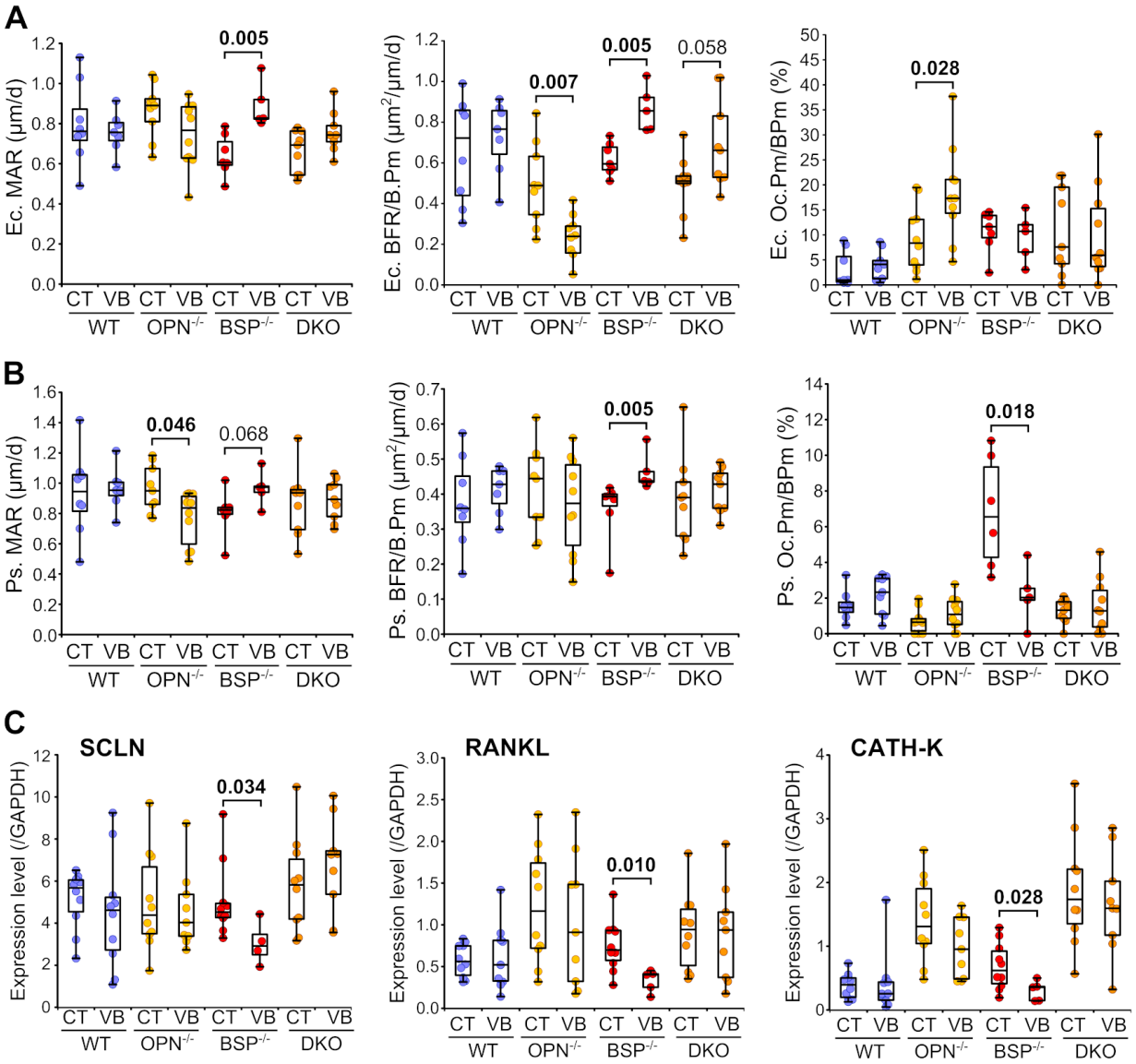

Maalouf et al., Figure 5

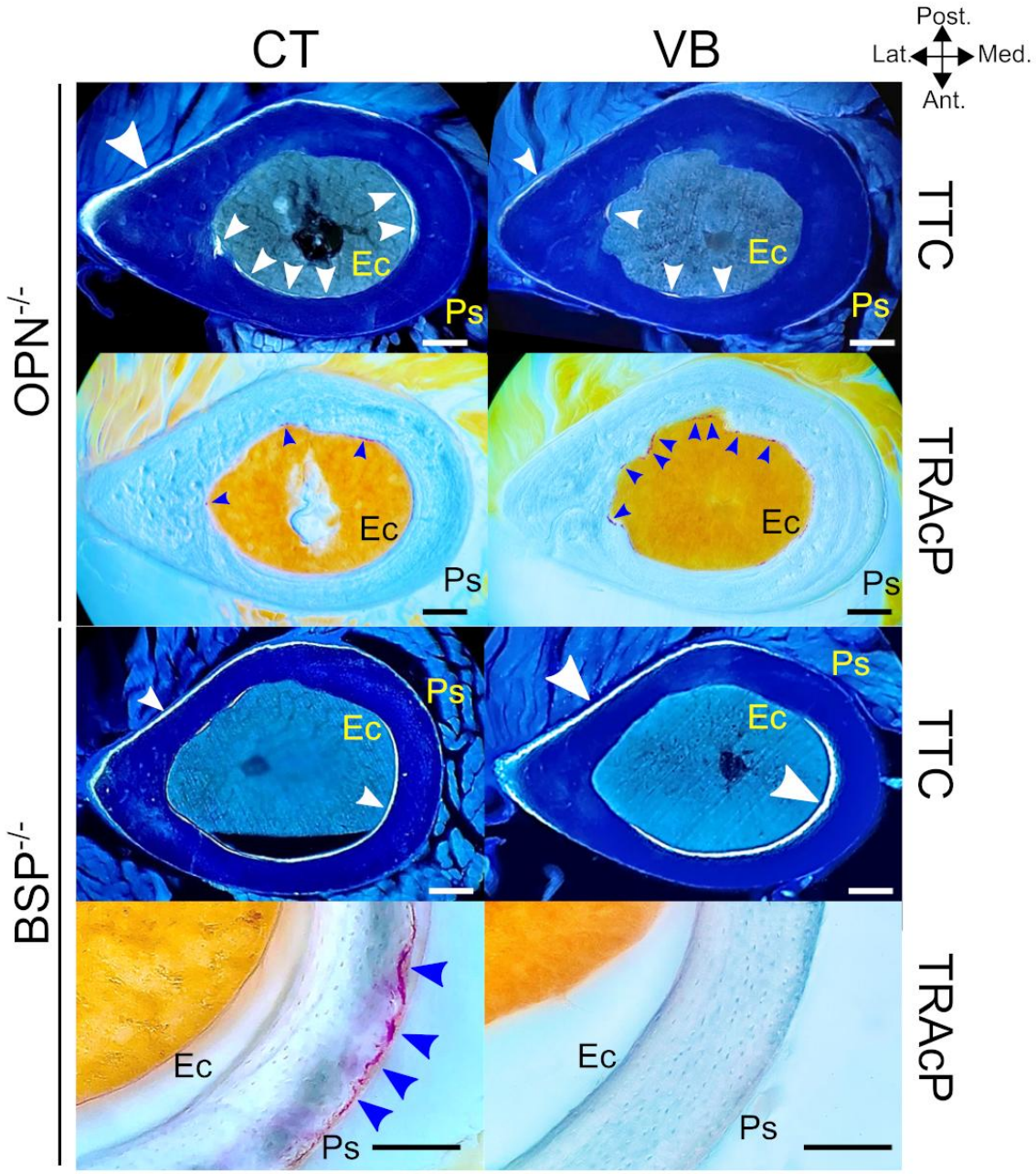

Maalouf et al., Figure 6